Metabolism 168 (2025) 156238

Contents lists available at ScienceDirect

Metabolism

journal homepage: www.journals.elsevier.com/metabolism

L-Kynurenine activates the AHR-PCSK9 pathway to mediate the lipid metabolic and ovarian dysfunction in polycystic ovary syndrome

Yujiao Wang [a,b], Yifan Wu [a,b], Hongwei Jiang [c], Shang Li [a,b], Jingjing Li [d], Cong Wang [a,b], Lexin Yang [a,b], Xiying Zhou [a,b], Juanjuan Yu [a,b], Junyu Zhai [a,b], Zi-Jiang Chen [a,b,e,f], Yanzhi Du [a,b,*]

[a] Center for Reproductive Medicine, Ren Ji Hospital, School of Medicine, Shanghai Jiao Tong University, Shanghai 200135, China
[b] Shanghai Key Laboratory for Assisted Reproduction and Reproductive Genetics, Shanghai 200135, China
[c] Luoyang Key Laboratory of Clinical Multiomics and Translational Medicine, Key Laboratory of Hereditary Rare Diseases of Health Commission of Henan Province, Henan Key Laboratory of Rare Diseases, Endocrinology and Metabolism Center, The First Affiliated Hospital, and College of Clinical Medicine of Henan University of Science and Technology, Luoyang 471003, China
[d] Department of Obstetrics and Gynecology, The First Affiliated Hospital, and College of Clinical Medicine of Henan University of Science and Technology, Luoyang 471003, China
[e] Center for Reproductive Medicine, Shandong University, National Research Center for Assisted Reproductive Technology and Reproductive Genetics, Key Laboratory of Reproductive Endocrinology of Ministry of Education, Shandong Provincial Key Laboratory of Reproductive Medicine, Jinan, Shandong 250012, China
[f] NMU-SD Suzhou Collaborative Innovation Center for Reproductive Medicine, China

ARTICLE INFO

Keywords:
Polycystic ovary syndrome
Dyslipidemia
L-Kynurenine
Epacadostat
Pyridoxal 5′-phosphate

ABSTRACT

Dysregulated amino acid metabolism is a key contributor to polycystic ovary syndrome (PCOS). This cross-sectional study revealed that serum levels of L-kynurenine (L-Kyn) were significantly elevated in women with PCOS, whereas pyridoxal 5′-phosphate (PLP) levels were markedly reduced. Moreover, human serum L-Kyn levels exhibited a positive correlated with low-density lipoprotein cholesterol (LDL-C) and a negative correlation with high-density lipoprotein cholesterol (HDL-C). Additionally, letrozole (LET) induced PCOS-like mice displayed increased hepatic L-Kyn levels. Mechanistically, both in vivo and in vitro experiments demonstrated that the upregulation of indoleamine 2,3-dioxygenase (IDO1) activates the aryl hydrocarbon receptor (AHR) - proprotein convertase subtilisin/kexin type 9 (PCSK9) pathway in the liver of PCOS-like mice, thereby contributing to dyslipidemia. Treatment with epacadostat, an inhibitor of the enzyme IDO1, or PLP, a cofactor for L-Kyn catabolism, effectively restored ovarian function, improved glucose tolerance, and ameliorated lipid profile abnormalities in PCOS-like mice.

1. Introduction

PCOS is a multifaceted metabolic and reproductive disorder affecting up to 18 % of women and its prevalence is surging [1,2]. PCOS is characterized by irregular ovulation, hyperandrogenism, and polycystic ovarian morphology [3,4]. Women with PCOS are predisposed to long-term metabolic consequences, including type 2 diabetes, insulin resistance (IR), dyslipidemia, non-alcoholic fatty liver disease (NAFLD), and cardiovascular disease [5–7]. Despite the significant heterogeneity in clinical manifestations among individuals, dyslipidemia is intrinsically linked to the pathogenesis of PCOS, which has been considered a metabolic hallmark of PCOS, affecting 50 % to 70 % of women with PCOS worldwide [8]. Adolescent girls with a familial predisposition to PCOS exhibit higher serum LDL-C, total cholesterol (TC), and triglycerides (TG) levels [9]. Recent evidence reveals that dyslipidemia associated with PCOS not only serves as an indicator of future dysfunction but also reflects underlying etiologies that drive long-term disease progression [10–12]. Hence, elucidating the molecular mechanisms underlying dyslipidemia in PCOS individuals is of significant scientific and clinical interest.

Emerging evidence has indicated that dynamic alterations in metabolite profiles display a leading risk factor for numerous metabolic diseases including PCOS [13–15]. Several studies have demonstrated aberrant metabolite composition in women with PCOS, such as bile

* Corresponding author at: 845 Lingshan Road, Shanghai 200135, China.
E-mail address: duyz@sjtu.edu.cn (Y. Du).

https://doi.org/10.1016/j.metabol.2025.156238
Received 31 January 2025; Accepted 21 March 2025
Available online 31 March 2025

acids (BAs), short-chain fatty acids (SCFAs), and branched-chain amino acids (BCAAs), aggravating inordinate glucose-lipid metabolism [15–17]. Our recent findings indicate that exposure to constant darkness induces metabolite alterations, contributing to the metabolic and reproductive hallmarks of PCOS in a rat model [8]. Gut microbiota-derived metabolite capric acid has been shown to inhibit hepatic galanin receptor 1 (GALR1), thereby impairing hepatic lipid metabolism in circadian disruption-induced PCOS rats. Untargeted metabolomics has identified a significant reduction in 3-Indoleacetic acid (IAA), a tryptophan (Trp) metabolite, in the stool of the PCOS-like rat model [8]. A cross-sectional study has also discovered abnormal Trp metabolism patterns in the plasma of PCOS patients [18]. However, the precise mechanism underlying the interplay between Trp metabolites and PCOS pathophysiology remain unclear.

Trp is an essential amino acid metabolized through three pathways: (I) conversion into indole and its derivatives by the gut microbiota; (II) catalyzed by IDO1 to Kyn; (III) hydroxylation by hydroxylase 1 to generate 5-hydroxytryptamine [19]. Dysregulation of these three metabolic pathways contributes to various diseases [20,21]. The Kyn pathway (KP), accounting for approximately 95 % of Trp metabolism, influences several pathophysiological processes by regulating inflammatory responses, metabolic disorders, and neurological functions [22,23]. Physical exercise training alleviates depression by regulating the balance of plasma and brain L-Kyn and kynurenic acid (Kyna) through the activation of peroxisome proliferator-activated receptor γ coactivator-1α (PGC-1α) and peroxisome proliferator-activated receptor α (PPARα) in the skeletal muscle of mice [24]. There is feasible evidence that gestational IR is mediated by the increased L-Kyn levels induced by the gut microbiome - IDO1 axis [25]. Overexpressed IDO1 in mature adipocytes from white adipose tissue (WAT) acts as the primary headstream of increased circulating L-Kyn in subjects with obesity and further causes IR through distinct signal transducer and activator of transcription 3 (STAT3)-interleukin-6 (IL6) signal pathway [3]. Yet, limited research has explored potential interventions targeting L-Kyn-mediated PCOS pathogenesis. And there is little evidence of Trp metabolite functions on reproductive and metabolic hemostasis in women. Hence, conducting this research to provide a theoretical foundation for the clinical management of PCOS is essential.

Herein, we investigated the impact of L-Kyn on dyslipidemia in patients with PCOS and a LET-induced PCOS-like mouse model, exploring the potential underlying mechanisms. The metabolomics results revealed that L-Kyn levels increased in the serum of PCOS patients than subjects without PCOS, which positively correlated with LDL-C concentrations and inversely correlated with HDL-C levels, and was consistently increased in the liver of PCOS mice. Furthermore, we demonstrated that the administration of L-Kyn in mice led to the manifestation of PCOS-like traits. The liver was identified as the target organ affected by L-Kyn, which impairs LDL-C clearance through the AHR-PCSK9 pathway in LET-induced PCOS-like mice. This is the first study to prove that epacadostat or PLP mitigates PCOS traits in mice. This study illuminates a novel mechanism underlying PCOS pathogenesis and proposes a potential therapeutic strategy for future clinical applications.

2. Results

2.1. Reproductive and metabolic phenotypes in LET-induced PCOS-like mouse model

To better clarify the mechanism driving the metabolic and reproductive dysfunctions in PCOS, we established a PCOS-like mouse model through successive subcutaneous LET injection, hereinafter defined as LET mice (Fig. 1a). The successful establishment of the PCOS-like mouse model was validated by key phenotypic hallmarks, including disrupted estrous cycles (Fig. 1b, c), ovarian polycystic changes manifested as decreased corpus luteum (CL) and increased atretic and cystic follicles (Fig. 1d), along with elevated serum testosterone (T) levels (Fig. 1e). Metabolic measurements exhibited that LET mice gained higher body weight (Fig. 1f) and had impaired glucose tolerance (Fig. 1g, h). Notably, LET-induced dyslipidemia was evident, as indicated by elevated serum LDL-C and reduced HDL-C levels (Fig. 1i). However, no significant differences were observed between the two groups in TG or TC levels. Furthermore, LET mice displayed pronounced exhibited obvious hepatic steatosis (Extended Data Fig. 1a). Oil Red O staining revealed that LET promoted hepatic lipid accumulation (Fig. 1j), coupled with adipocyte hypertrophy (Fig. 1l). Additionally, transmission electron microscopy scans further confirmed hepatic steatosis in PCOS mice, characterized by an increased lipid droplet deposition, mitochondrial swelling with irregular morphology, and disrupted cristae structure (Fig. 1k), suggest enhanced lipogenesis. Collectively, disrupted ovarian function and changes in lipid-modifying target organs were observed in LET-induced PCOS mice. However, whether these effects are causal is still controversial. This triggers further investigation into this question.

2.2. Tissue-specific L-Kyn changes in LET-induced PCOS-like mouse model

Metabolites play a pivotal role in the pathogenesis of PCOS. Our previous study identified the interplay between lipid dysmetabolism and microbiome-metabolome in a circadian disruption-induced PCOS-like rat model [8]. One of the Trp metabolites, IAA, was observed to be reduced in this kind of PCOS-like model. Evidence suggests that circulating L-Kyn levels increased in obese subjects [3]. Therefore, major metabolic tissues, including fat tissue, liver, skeletal muscle (SK), and serum were collected to Trp and its downstream intermediates determination by liquid chromatography-tandem mass spectrometry (LC-MS) analysis (Fig. 2a, b). Metabolite assays revealed dysregulation of the KP in PCOS mice, despite unchanged Trp levels (Fig. 2d, e). Indeed, a remarkable increase in L-Kyn levels and the L-Kyn to Trp ratio (KTR) were observed exclusively in the liver tissue of the PCOS group (Fig. 2e, f). However, there was no significant difference of L-Kyn levels in the SK and fat tissue between the control and LET groups. Moreover, liver serotonin levels displayed a decreasing trend in the LET group compared to the controls (Fig. 2g), although the statistical analysis was not significant. Furthermore, there were no changes in IAA levels in the PCOS mice compared with the control group (Fig. 2h). This indicates that Trp catabolism was directed toward the KP pathway. These data indicate that the liver, as opposed to other metabolite organs, primarily influences Trp metabolism, favoring the KP pathway over the pathways involving indole and serotonin. Since L-Kyn is a Trp downstream catalyzed by IDO1. An elevated KTR indicates a substantial increase in IDO1 activity. To further elucidate the role of L-Kyn in PCOS, we employed epacadostat, a potent and selective IDO1 inhibitor, in rescue experiments. Interestingly, epacadostat administration significantly reduced L-Kyn levels and KTR in the liver of PCOS mice without affecting L-Kyn content in fat tissue and SK (Fig. 2e, f). These findings support the hypothesis that L-Kyn contributes to PCOS pathogenesis by targeting the liver tissue.

2.3. Epacadostat exerts an inhibitory effect against PCOS-like symptoms by regulating IDO1 expression

Liver L-Kyn levels were elevated, accompanied by a rising trend in KTR, indicating a substantial upregulation of IDO1 under LET induction. This prompted us to hypothesize that IDO1 activation could be responsible for the characteristics of PCOS mice. Therefore, we assessed the expression of IDO1 and other enzymes involved in Trp metabolism. The expression of Ido1 overexpression at the mRNA and protein levels in the liver tissue of the LET group (Fig. 3a, b, c). However, RT-qPCR analysis displayed no significant differences in the expression of other Trp metabolism-related enzymes, including *kynurenine-3-*

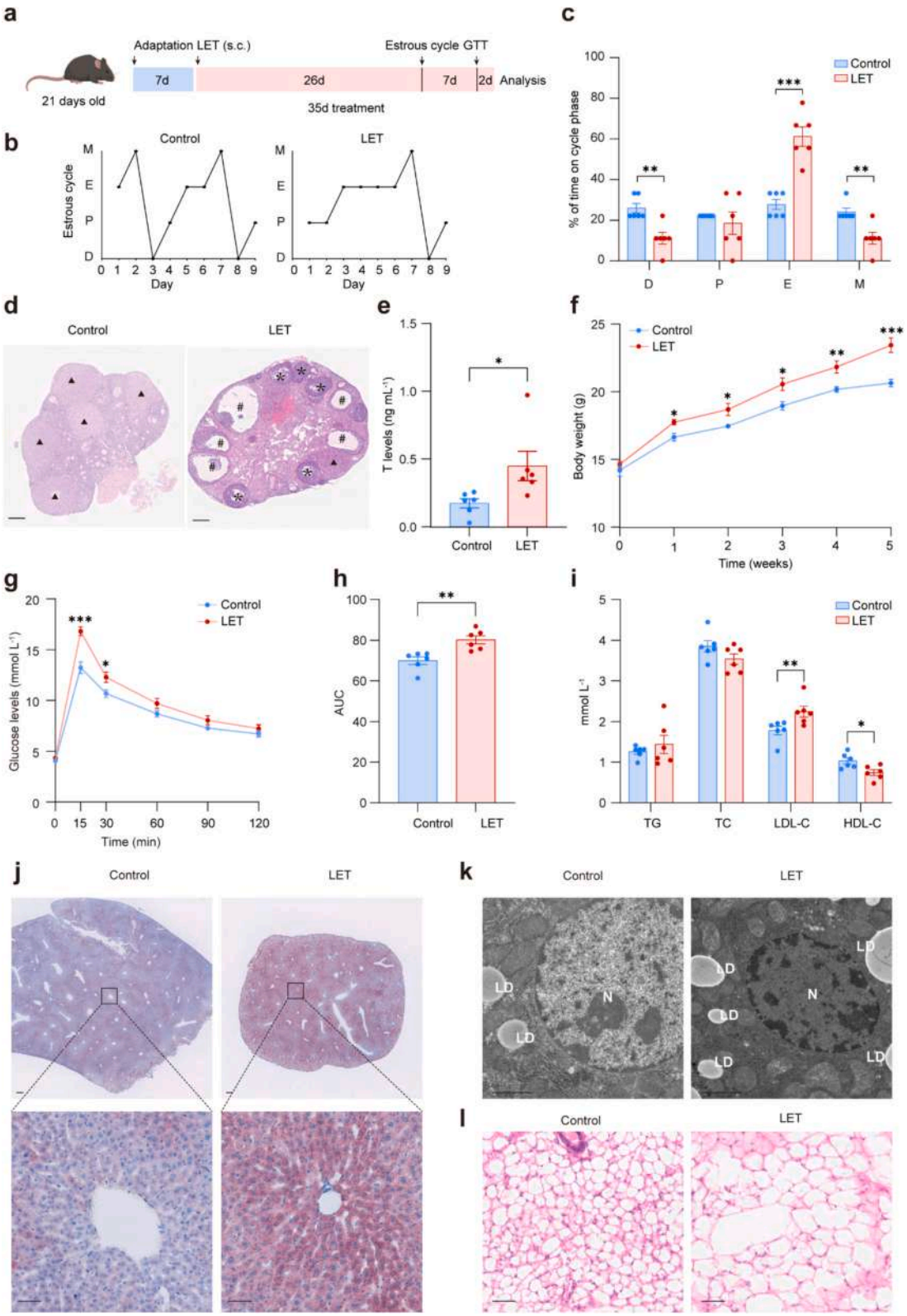

Fig. 1. Ovarian dysfunction and metabolic disturbance in LET-induced PCOS mice. a, Schematic illustration of the mice model design. The mice were divided into two groups. The mice were treated for 35 days with PBS as the control group or LET as the LET group. b, Representative estrous cycles. M, metestrus; D, diestrus; P, proestrus; E, estrus. c, Percentage of each stage in estrous cycles (n = 6 mice per group). d, Ovary morphology represented by HE staining. The triangle symbol represents CL; The asterisk symbol represents atretic follicles; The well number symbol represents cystic follicles. Scale bar: 200 μm. e, Measurement of serum T levels (n = 6 mice per group). f, Body weight changes (n = 6 mice per group). g, h, Glucose tolerance tests (GTT) and area under the curve (AUC) (n = 6 mice per group). i, Serum lipid content (n = 6 mice per group). j, Representative Oil Red O staining of livers. Scale bar: 200 μm and 50 μm. k, Representative images of liver ultrastructure detected by transmission electron microscope. Scale bar: 2 μm. LD represents the lipid droplet; N represents the nucleus. l, Representative HE staining images of WAT. Scale bar: 50 μm. *p* values were determined by unpaired *t*-tests and data were presented as means ± SEM. $^{*}p < 0.05$; $^{**}p < 0.01$; $^{***}p < 0.001$ LET versus the control.

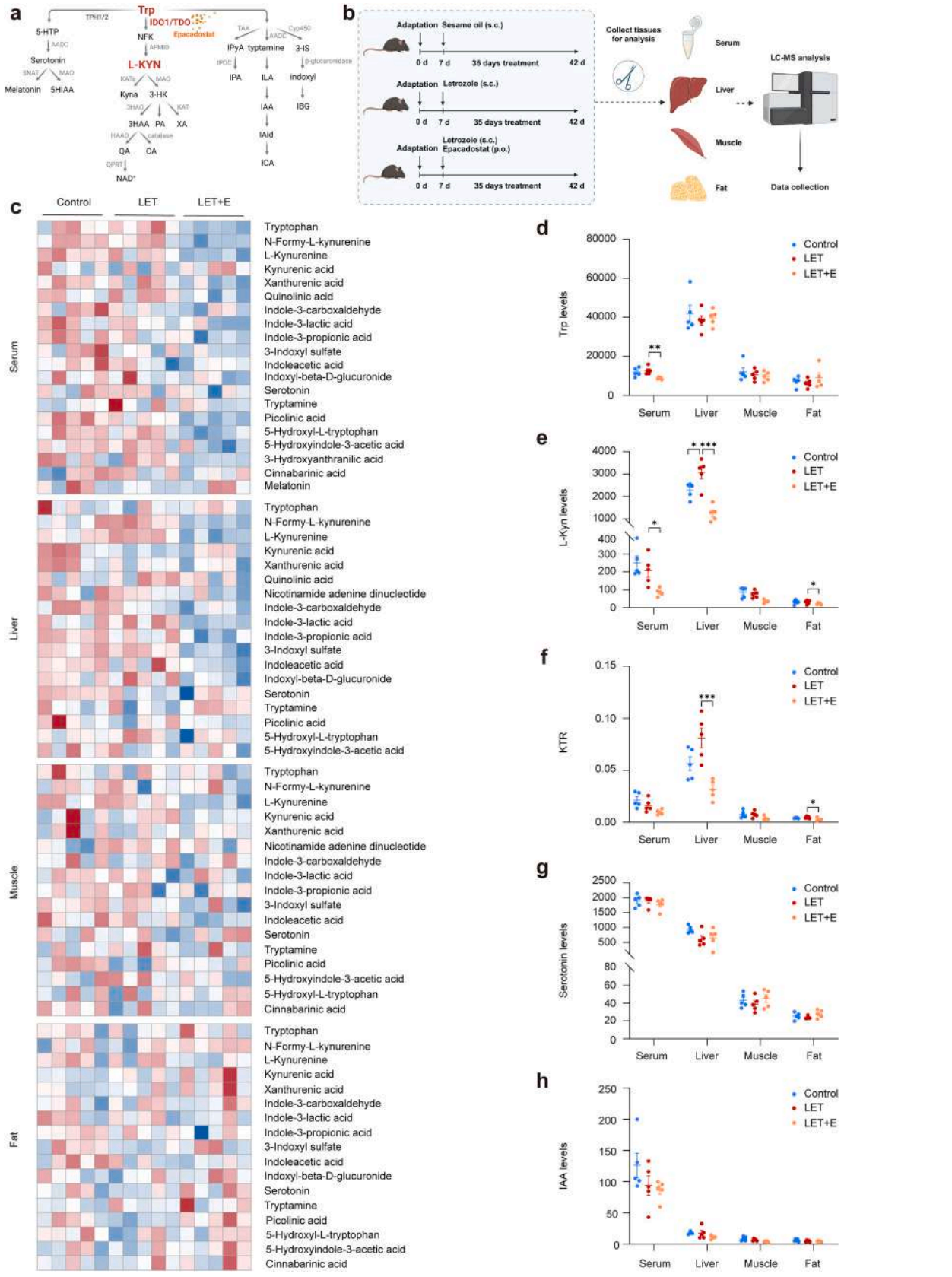

(caption on next page)

Fig. 2. Metabolite profiles of Trp metabolism in serum, liver, muscle, and fat tissue of mice. a, Pathway of Trp metabolism. b, Schematic illustration of the mice model design. The mice were divided into three groups. The mice were treated for 35 days with PBS as a control group or LET as the LET group. The mice in the LET+E group received both LET and epacadostat simultaneously. c, Heat map of Trp metabolites in serum, liver, muscle, and fat tissue from each group (n = 5 mice per group). d, Quantitative analysis of Trp levels (n = 5 mice per group). e, Quantitative analysis of L-Kyn levels (n = 5 mice per group). f, Quantitative analysis of KTR (n = 5 mice per group). g, Quantitative analysis of serotonin levels (n = 5 mice per group). h, Quantitative analysis of IAA levels (n = 5 mice per group). The units of these substances are expressed in ng mL^{-1} in serum, and in ng g^{-1} in liver, SK, and fat tissue. *p* values were determined by one-way ANOVA with Tukey's multiple comparison post-hoc test and data were presented as means ± SEM. $^{*}p < 0.05$; $^{**}p < 0.01$; $^{***}p < 0.001$. Tryptophan hydroxylase, TPH; 5-Hydroxytryptophan, 5-HTP; Aromatic amino acid decarboxylase, AADC; Monoamine oxidase, MAO; 5-Hydroxyindole-3-acetic acid, 5-HIAA; Serotonin *N*-acetyltransferase, SNAT; N-Formy-L-kynurenine, NFK; Arylformamidase, AFMID; Kynurenine aminotransferase, KAT; 3-hydroxykynurenine, 3-HK; 3-hydroxyanthranilic acid, 3, 4-dioxygenase, 3HAO; 3-hydroxyanthranilic acid, 3-HAA; Xanthurenic acid, XA; Picolinic acid, PA; 3-Hydroxyanthranilate 3,4-dioxygenase, HAAO; Quinolinic acid, QA; Quinolate phosphoribosyltransferase, QPRT; Cinnabarinic acid, CA; Tryptophan aminotransferase, TAA; Indole-3-pyruvic acid, IPyA; Indole-3-pyruvate decarboxylase, IPDC; Indole-3-propionic acid, IPA; Phenylpyruvate dehydrogenase, PPDH; Indole-3-aldehyde, IAId; Indole-3-carboxaldehyde, ICA; Cytochrome P450, Cyp450; 3-Indoxyl sulfate, 3-IS; Indoxyl-beta-D-glucuronide, IBG.

monooxygenase (*Kmo*), kynurenine aminotransferase 1 (*Kat1*), kynurenine aminotransferase 2 (*Kat2*), and kynurenine aminotransferase 3 (*Kat3*) (Fig. 3a). Furthermore, serum levels of interferon-gamma (ifnγ), the main inducer of IDO1, significantly elevated in PCOS-like mice (Fig. 3d), along with a significant upregulation of *Ifnγ* mRNA expression in the liver tissue (Fig. 3e). Notably, epacadostat treatment restored the disrupted estrous cycle (Fig. 3f, g) and ovary morphology (Fig. 3h) in PCOS mice by suppressing Ido1 expression. Also, epacadostat significantly ablated the elevated serum T levels in PCOS mice (Fig. 3i). Metabolic measurements demonstrated that epacadostat also attenuated body weight gain (Fig. 3j) and ameliorated impaired glucose tolerance (Fig. 3k, l, and Extended Data Fig. 2a). Upon analysis of the lipid profiles, epacadostat administration lowered LDL-C levels but had no effect on TG or TC levels in mice who received LET induction (Extended Data Fig. 2b). Additionally, epacadostat had no use in improving the HDL-C levels of PCOS mice. Moreover, epacadostat protected the mice from excessive hepatic lipid accumulation (Extended Data Fig. 2c), as shown by Oil Red O staining and transmission electron microscopy (Fig. 3m, n). Similarly, epacadostat reduced adipocyte hypertrophy in PCOS mice (Fig. 3o). These findings suggest that inhibiting IDO1 protects against LET-induced reproductive and metabolic abnormalities of PCOS by limiting L-Kyn production.

2.4. PCOS characteristics depend on L-Kyn in PCOS patients and PCOS-like mice

The dysregulated Trp metabolism in PCOS mice prompted us to explore the correlation between L-Kyn and the PCOS indices. We recruited a cohort of 84 participants, comprising 44 controls and 40 individuals diagnosed with PCOS (Fig. 4a). Extended Data Table 1 presents the demographic characteristics and laboratory data of controls and women with PCOS, including age, BMI, reproductive index, and serum lipid profile. Compared to the control group, women with PCOS exhibited significantly higher levels of luteinizing hormone (LH), T, AMH, and TG, which were in accordance with the characteristics of endocrine and metabolic disorders in PCOS. Although the age distribution significantly differed between the two groups, this discrepancy resulted from the lack of age matching. Indeed, we conducted an analysis of covariance (ANCOVA) to examine the relationship between age and L-Kyn levels and found that age does not influence L-Kyn levels. LC-MS assay indicated no significant differences in serum Trp and L-Kyn levels between PCOS patients and controls (Fig. 4b, c). However, when stratifying patients into four BMI-based groups, we observed a notable elevation in serum L-Kyn levels in overweight PCOS patients (Fig. 4d). Consistent with L-Kyn levels, the KTR ratio was also higher in obese PCOS patients (Fig. 4e, f). We further visualized the correlation between serum L-Kyn levels and metabolic parameters using Spearman correlation analysis. The results showed that L-Kyn levels positively correlated with LDL-C levels ($r = 0.2512$, $p = 0.0212$) (Fig. 4g). In contrast, L-Kyn levels were inversely associated with HDL-C levels ($r = -0.2726$, $p = 0.0121$) (Fig. 4h) and showed no significant relationship with TG ($r = 0.0803$, $p = 0.4681$) or TC ($r = 0.0579$, $p = 0.6011$) (Fig. 4i, j). Based on these results, we deduce that L-Kyn contributes to lipid metabolism dysregulation in PCOS, particularly in overweight patients.

The next critical question is whether the PCOS-like phenotype induced by LET depends on L-Kyn levels. We then subcutaneously administered LET or L-Kyn (20 mg kg^{-1} d^{-1}) to mice for 35 consecutive days (Fig. 4k). As expected, L-Kyn renders the mice with PCOS traits similar to the LET group, as evidenced by abnormal estrous cycle (Extended Data Fig. 3a) and polycystic ovary morphology like the LET group (Extended Data Fig. 3b). Interestingly, L-Kyn had a minor impact on T levels (Fig. 4l). Likewise, no positive correlation was observed between L-Kyn levels and T levels in patients (Extended Data Fig. 3e). Compared to the controls, exogenous L-Kyn rendered mice with higher body weight (Fig. 4m) and aggravated glucose tolerance, mirroring phenotypes seen in LET-induced PCOS mice (Fig. 4n, o, and p). L-Kyn also triggers hepatic steatosis (Extended Data Fig. 3c) and adipocyte hypertrophy (Extended Data Fig. 3d). Furthermore, L-Kyn increased serum LDL-C levels but did not affect TC, TG, or HDL-C levels (Extended Data Fig. 3f). These findings suggest that L-Kyn plays an essential role in the development of PCOS. To further validate the role of L-Kyn in PCOS pathogenesis, we conducted the following experiments in *Ido1* knockout mice (Fig. 4k, q, and Extended Data Fig. 3g). As expected, $Ido1^{-/-}$ mice exhibited resistance to LET-induced PCOS-like manifestations, maintaining reproductive and metabolic parameters comparable to controls (Extended Data Fig. 3a, b, c, d, h, i, and j). Furthermore, the characteristics of PCOS recur in $Ido^{-/-}$ knockout mice when they are injected with both LET and L-Kyn simultaneously. Collectively, these findings suggest that L-Kyn plays a key role in the pathogenesis of PCOS.

2.5. L-Kyn exacerbates dyslipidemia via AHR-PCSK9 axis in PCOS

Emerging evidence suggests that liver dysfunction, particularly NAFLD and dyslipidemia, constitutes a major metabolic manifestation of PCOS. Abnormal lipid metabolism are intricately linked to the local microenvironment of follicular fluid and steroid hormone in the ovary [26]. However, the precise mechanisms underlying this interplay in PCOS remain poorly understood. The above results revealed a positive correlation between L-Kyn and LDL-C levels in patients, as well as a significant reduction of LDL-C levels in PCOS mice with *Ido1* inhibition or deficiency (Fig. 4g, Extended Data Fig. 2b, and Extended Data Fig. 3i). Accordingly, to elucidate the exact mechanism by which L-Kyn affects lipid metabolism, we first assessed the expression of PCSK9, a key regulator of LDL-C regradation [27]. The results showed a significant upregulation of PCSK9 at both mRNA expression and protein levels in the liver of LET mice, which was reversed upon Ido1 inhibition by epacadostat (Fig. 5a, b).

To investigate the cellular pathways responsible for abnormal hepatic lipid accumulation, we treated HepG2 cells with a range of concentrations of L-Kyn (0, 62.5, 125, 250, 500, 1000 μg mL^{-1}). Cell viability results are presented in Extended Data Fig. 4a. Based on this result, we selected the intermediate concentration (250 μg mL^{-1} L-Kyn) for the subsequent study. Oil Red staining revealed that L-Kyn stimulation let to increased lipid accumulation (Fig. 5c). Subsequent qRT-PCR

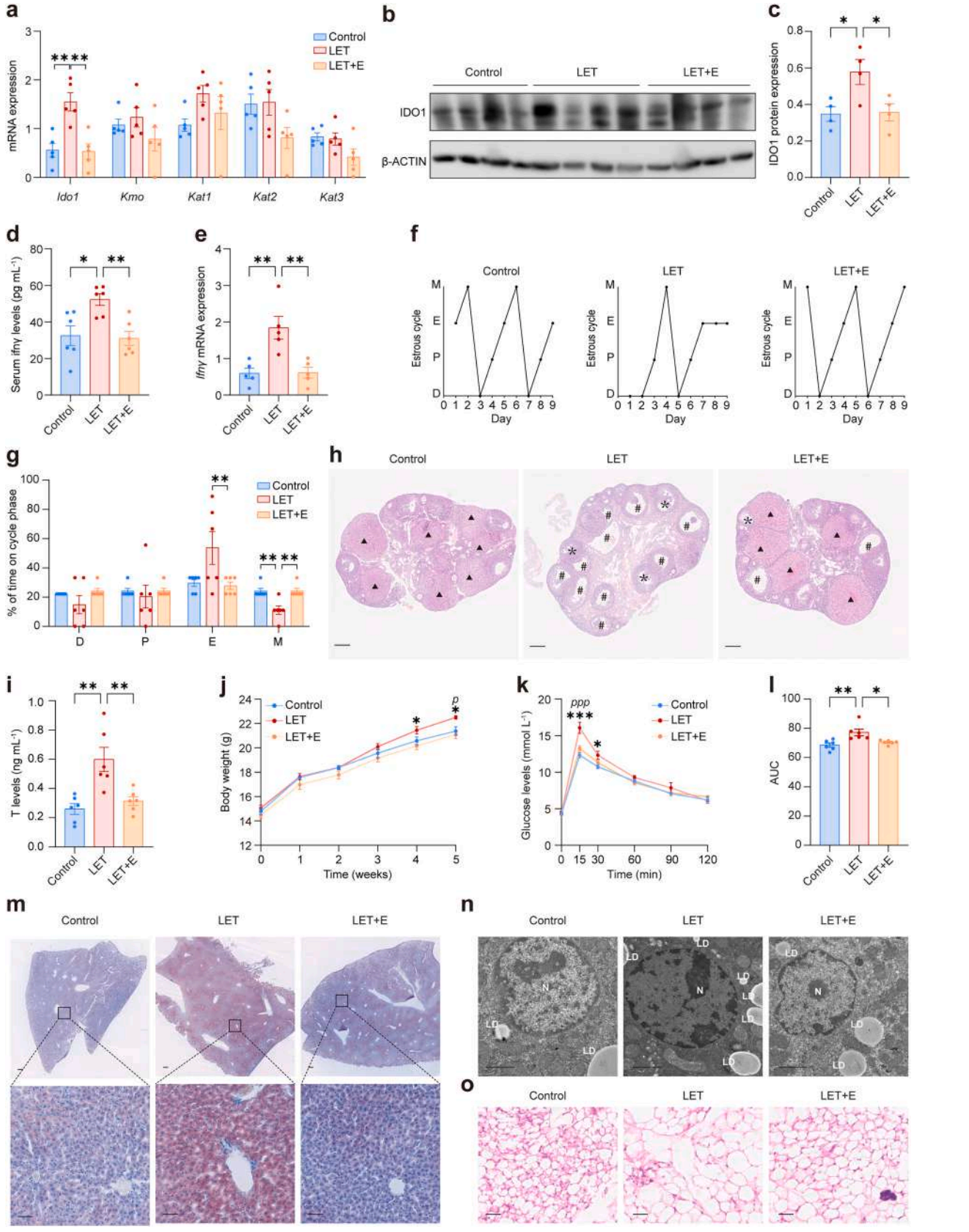

(caption on next page)

Fig. 3. Epacadostat supplementation ameliorates reproductive index and dyslipidemia in LET-induced PCOS-like mice. a, Relative mRNA expressions related to Trp metabolism-related enzymes of liver from mice in the indicated groups (n = 5 mice per group). b, c, The protein levels of IDO1 in the liver of mice from the indicated groups (n = 4 mice per group). d, Quantities of serum ifnγ levels (n = 6 mice per group). e, Relative *Ifnγ* mRNA expressions in the liver of mice from the indicated groups (n = 5 mice per group). f, Representative estrous cycles. M, metestrus; D, diestrus; P, proestrus; E, estrus. g, Percentage of each stage in estrous cycles (n = 6 mice per group). h, Ovary morphology represented by HE staining. The triangle symbol represents CL; The asterisk symbol represents atretic follicles; The well number symbol represents cystic follicles. Scale bar: 200 μm. i, Measurement of serum T levels (n = 6 mice per group). j, Body weight changes (n = 6 mice per group). k, l, GTT and AUC (n = 6 mice per group). m, Representative Oil Red O staining of livers. Scale bar: 200 μm and 50 μm. n, Representative images of liver ultrastructure detected by transmission electron microscope. Scale bar: 2 μm. LD represents the lipid droplet; N represents the nucleus. o, Representative HE staining images of WAT. Scale bar: 50 μm. For a, c, d, e, g, i, and l, *p* values were determined by one-way ANOVA with Tukey's multiple comparisons post-hoc test, and data were presented as means ± SEM. $^{*}p < 0.05$; $^{**}p < 0.01$; $^{***}p < 0.001$. For j and k, *p* values were determined by one-way ANOVA with Tukey's multiple comparisons post-hoc test, and data were presented as means ± SEM. $^{*}p < 0.05$; $^{**}p < 0.01$; $^{***}p < 0.001$, Control versus the LET group. $^{p}p < 0.05$; $^{pp}p < 0.01$; $^{pp}p < 0.001$, LET versus the LET+E group.

analysis confirmed that L-Kyn stimulation triggers a significant upregulation of *PCSK9* in HepG2 (Fig. 5d). Correspondingly, adding L-Kyn to HepG2 cells distinctly increased the protein levels of PCSK9 (Fig. 5e, f). L-Kyn is known to activate the AHR, which subsequently translocates to the nucleus, dimerizes with the aryl hydrocarbon receptor nuclear translocator (ARNT), and regulates downstream gene transcription [21,28]. Western blot analysis confirmed that L-Kyn stimulation increased AHR expression in HepG2 (Fig. 5e, g). To explore the interaction between L-Kyn and AHR, we used CB-DOCK, a precise protein-ligand blind docking tool. The successful docking of L-KYN and AHR is illustrated in Fig. 5h. Based on these results, we hypothesize that L-Kyn exacerbates dyslipidemia through the AHR-PCSK9 axis. To test this hypothesis, we conducted a rescue experiment by co-treating HepG2 with L-Kyn and StemRegenin 1 (SR1), an AHR inhibitor. SR1 treatment effectively reduced PCSK9 by inhibiting AHR expression (Fig. 5d, e, f, and g). Notably, inhibition of AHR by SR1 also mitigated lipid accumulation in the L-Kyn-treated HepG2 cells (Fig. 5c). We then evaluated the effect of L-Kyn on LDL-C function using a DiI-LDL uptake assay, where the fluorescence in HepG2 cells reflects their ability to absorb LDL-C. The results shown in Fig. 5i demonstrated that L-Kyn could enhance LDL-C uptake, while AHR inhibition by SR1 attenuated this effect. Given the important roles of PCSK9 in regulating LDL-C levels, these findings suggest that L-Kyn modulates lipid metabolism in PCOS by upregulating PCSK9 via AHR activation.

2.6. PLP ameliorates PCOS by promoting L-Kyn catabolite to Kyna

PLP, the active form of vitamin B6, functions as an important coenzyme in numerous enzymatic reactions, including amino acid metabolism, neurotransmitter synthesis, heme production, and other physiological functions [29]. Additionally, PLP serves as a cofactor for key enzymes involved in converting L-Kyn to Kyna (Fig. 6a). We evaluated B-group vitamins, including PLP, in the serum of controls and women with PCOS. Among these vitamins, serum PLP levels were lower in the PCOS group as compared to the controls (Fig. 6b to i). No statistically significant differences were observed in the levels of other B-group vitamins (VitB1, VitB2, VitB3, VPP, VitB6, and VitB7) between the two groups. Interestingly, VitB5 levels were higher in the PCOS group. Given the enzymatic role of PLP in L-Kyn metabolism, we next quantified serum Kyna levels and found that PCOS patients exhibited decreased serum Kyna content compared to the control group (Fig. 6j). Next, we investigated the therapeutic effects of PLP by adding it to the drinking water of mice (Fig. 6k). Consistent with the results, Kyna levels were significantly reduced in the liver of the LET mice (Fig. 6l). There was a trend suggesting the levels of Kyna slightly increased following PLP administration although there was no significant difference. The ratio of L-Kyn to Kyna, an indicator of enzymatic activity involved in L-Kyn catabolism, significantly decreased in the liver of PCOS mice and was effectively restored after PLP supplementation (Fig. 6m). PLP administration successfully restored estrous cycles (Fig. 6n, o) and dramatically reduced cystic follicles in the ovaries (Fig. 6p). Furthermore, the beneficial effects of PLP extended to endocrine and metabolic parameters, as evidenced by a reduction in hyperandrogenism (Fig. 6q). Consistently, mice given PLP administration exhibited lower body weight (Fig. 6r), accompanied by improved glucose homeostasis (Fig. 6s, t and Extended Data Fig. 5a) and an improvement in serum LDL-C and TC levels (Extended Data Fig. 5b). Collectively, these findings highlight the pivotal role of aberrant L-Kyn metabolism in PCOS pathogenesis and underscore PLP as a promising therapeutic strategy for mitigating reproductive and metabolic disturbances in PCOS.

3. Discussion

Emerging evidence suggests that disrupted glucose and lipid metabolism contributed to the pathogenesis of PCOS. However, the role of amino acid metabolism in PCOS has been largely overlooked. Increasing evidence supports the role of bioactive compounds produced derived from amino in maintaining homeostasis across various physiological processes, such as inflammation, metabolism, immune responses, and nervous system function [30]. Recent advances highlight an intimate relationship between Trp metabolism and the progression of various diseases. Disruption in Trp metabolism has been implicated in conditions such as pregnancy IR, obesity, respiratory issues, vascular pathology, and depression [3,18,19,24,28,29]. Nevertheless, few clues have indicated the possible effect of Trp and its metabolites on PCOS intervention. A recent cross-sectional study found abnormal activation of the Trp pathway in PCOS patients [18]. However, the precise source of the Kyn and its function in PCOS remain unclear. Our previous findings revealed downregulation of the indole pathways of Trp catabolism in the circadian dysrhythmia-induced PCOS rat model [8], prompting further investigation into the role of Trp and its metabolites in PCOS development. In this study, we observed elevated serum L-Kyn levels in obese PCOS patients. Mechanistically, metabolomic analysis of tissues from the LET-induced PCOS mice model revealed that excessive L-Kyn, derived from the liver tissue, exacerbated higher levels of LDL-C through the AHR-PCSK9 pathway. Pharmacological intervention using the inhibitor epacadostat, or PLP, a coenzyme for KATs, demonstrated beneficial effects on reproductive endocrinology and metabolic homeostasis in PCOS-like mice, mitigating hyperandrogenism, irregular estrous cycles, polycystic ovarian morphology, higher body weight, impaired glucose tolerance, hepatic steatosis, and adipocyte hypertrophy.

To assess the impact of L-Kyn on PCOS pathogenesis, we first look for an accurate mouse model that mirrors PCOS traits. Previous studies have utilized estradiol valerate, dehydroepiandrosterone (DHEA), dihydrotestosterone (DHT), T, anti-mullerian hormone (AMH), human chorionic gonadotropin (hCG), and LET to conduct PCOS-like mice [4,16,27,31]. Notably, abnormal L-Kyn levels have been reported to accelerate the development of IR and obesity [3,25]. Given its comprehensive metabolic and reproductive phenotype, we utilized a LET-induced PCOS-like mice model in this study, as it exhibits elevated serum T levels, irregular estrous cycles, polycystic ovarian morphology, higher body weight, impaired glucose tolerance, hepatic steatosis, and adipocyte hypertrophy (Fig. 1b to l, Extended Data Fig. 1).

Trp is absorbed from dietary sources by the intestinal epithelium and transported via the bloodstream to distant target organs [19], where it

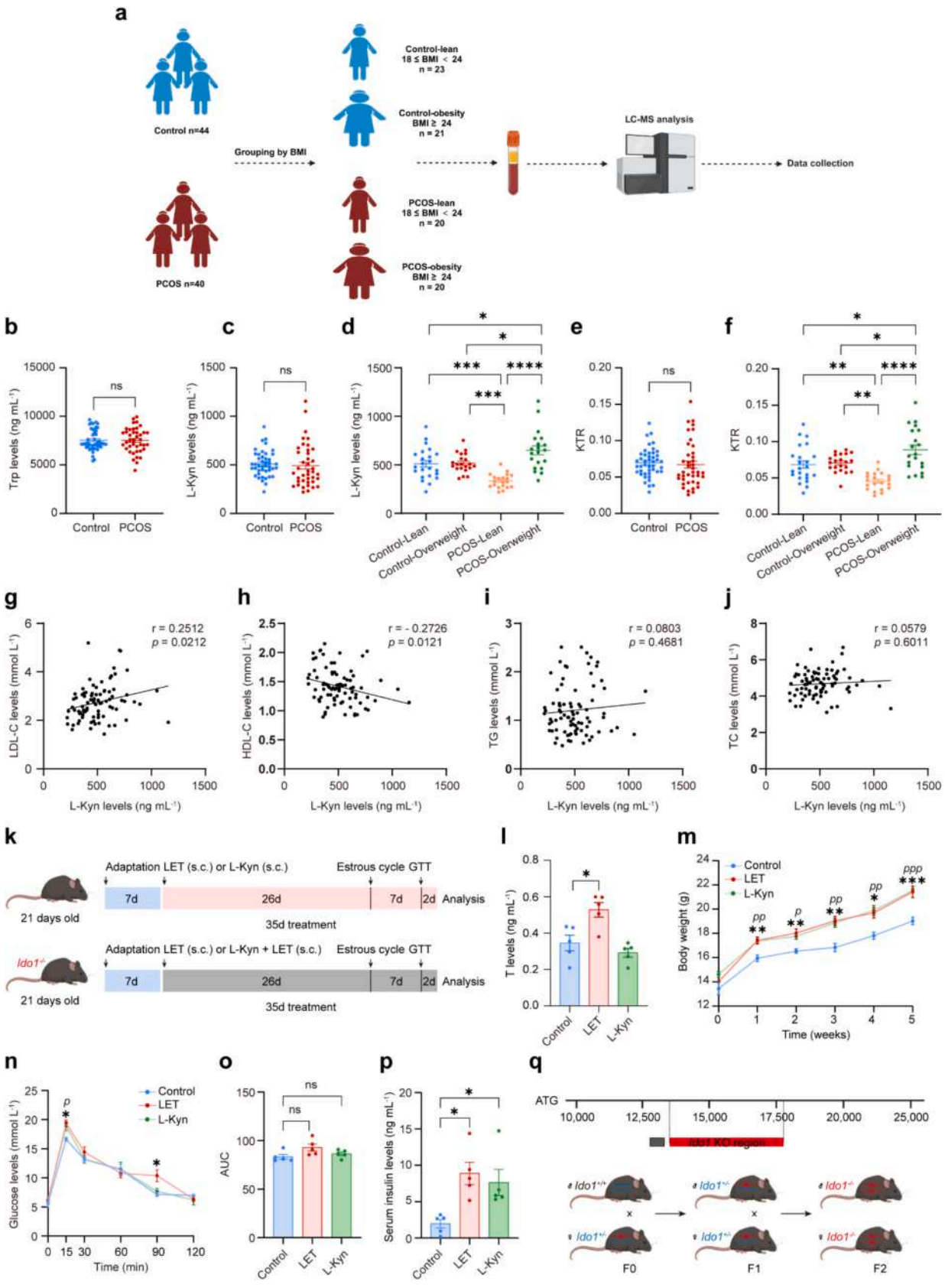

(caption on next page)

Fig. 4. Changes in the L-Kyn are associated with the dyslipidemia in PCOS. a, Flow chart depicting the patients grouping and serum Trp metabolites analysis. b, Serum Trp levels of female individuals with or without PCOS (n = 44 in the Control group, n = 40 in the PCOS group). c, Serum L-Kyn levels of female individuals with or without PCOS (n = 44 in the Control group, n = 40 in the PCOS group). d, Serum L-Kyn levels in Control-lean subjects (18 ≤ BMI < 24, n = 23), Control-overweight subjects (BMI ≥ 24, n = 21), PCOS-lean subjects (18 ≤ BMI < 24, n = 20) and PCOS-overweight subjects (BMI ≥ 24, n = 20). e, Serum KTR levels of female individuals with or without PCOS (n = 44 in the Control group, n = 40 in the PCOS group) f, Serum L-Kyn levels in Control-lean subjects (18 ≤ BMI < 24, n = 23), Control-overweight subjects (BMI ≥ 24, n = 21), PCOS-lean subjects (18 ≤ BMI < 24, n = 20) and PCOS-overweight subjects (BMI ≥ 24, n = 20). g, h, i, and j, Correlation analysis of serum L-Kyn levels with LDL-C, HDL—C, TG, and TC in patients (n = 84). k, Schematic illustration of the mice model design. The mice were divided into five groups: Control, LET, L-Kyn, *Ido1*$^{-/-}$ + LET, and *Ido1*$^{-/-}$ + L-Kyn + LET. The wild-type mice in the control group were treated with PBS for 35 days, while those in the LET group and L-Kyn group received LET or L-Kyn treatment for the same duration, respectively. The *Ido1*$^{-/-}$ mice were treated for 35 days with LET in the *Ido1*$^{-/-}$ + LET group, and with both L-Kyn and LET simultaneously in the *Ido1*$^{-/-}$ + L-Kyn + LET group. l, Measurement of serum T levels (n = 5 mice per group). m, Body weight changes (n = 5 mice per group). n, o, GTT and AUC (n = 5 mice per group). p, Serum insulin levels (n = 5 mice per group). q, The schedule of the population expansion of the *Ido1*$^{-/-}$ mice. For b, c, and e, *p* values were determined by the unpaired test. For d, f, l, o and p, *p* values were determined by one-way ANOVA with Tukey's multiple comparisons post-hoc test, and data were presented as means ± SEM. *$p < 0.05$; **$p < 0.01$; ***$p < 0.001$, ****$p < 0.0001$. For m and n, *p* values were determined by one-way ANOVA with Tukey's multiple comparisons post-hoc test, and data were presented as means ± SEM. *$P < 0.05$, **$p < 0.01$, ***$p < 0.001$, Control versus the LET group. $^{p}p < 0.05$, $^{pp}p < 0.01$, $^{ppp}p < 0.001$, Control versus the L-Kyn group.

undergoes metabolism through three major pathways: the KP, the serotonin pathway, and the indole pathway. The KP of Trp metabolism occurs predominantly in the liver, accounting for over 95 % of Trp is metabolized into bioactive compounds [19,32]. A small proportion of Trp is catalyzed to 5-hydroxytryptophan (5-HTP) by tryptophan hydroxylase (TPH), which is further decarboxylated by aromatic L-amino acid decarboxylase (AADC) to produce serotonin. Additionally, indole and its derivatives represent minor metabolic products of Trp metabolism. The liver, WAT, and SK play pivotal roles in maintaining reproductive and metabolic homeostasis in females [33]. Here, in virtue of LC-MS techniques to analyze Trp catabolites in serum, liver, fat tissue, and SK, we identified the liver as the primary site of excessive L-Kyn production in PCOS mice (Fig. 2e). Furthermore, we quantified key metabolites from the other two Trp metabolic pathways. Serotonin levels exhibited a slight decreasing trend in the liver of PCOS mice (Fig. 2g), consistent with a previous study reporting reduced serotonin levels in the hippocampal tissue of PCOS-like mice [34]. However, levels of IAA, a downstream metabolite of the indole pathway, showed no significant changes (Fig. 2h). Given that Trp availability is a limiting factor for its metabolic pathways, we hypothesize that an upregulation of one pathway may lead to a reduced flux in others. This metabolic imbalance may drive excessive KP activation, contributing to PCOS pathophysiology. Three key enzymes, tryptophan 2,3-dioxygenase (TDO), IDO1, and IDO2, catalyze the initial conn continues to degrade to Kyna catalyzed by the KATs. IDO1 and IDO2 are expressed in various organs, including the liver, gastrointestinal tract, kidney, and brain, whereas TDO is predominantly expressed in the liver. IDO1 overexpression has been observed in the small intestine, colon, and WAT of subjects with gestational diabetes mellitus (GDM) and obesity [3,25]. However, little research has explored IDO1 expression in PCOS. In our study, the comparative analysis of KP enzyme expression in the liver of PCOS-like mice revealed selective upregulation of IDO1, with a concomitant increase in ifnγ, the primary inducer of IDO1 (Fig. 3a, b, c, d, and e). Consistent with these results, IDO1 activity, as reflected by KTR, was slightly elevated in the liver of PCOS mice (Fig. 2f). IDO1 deserves to be a promising target for treating several disorders. Epacadostat, a potent selective IDO1 inhibitor, has demonstrated efficacy in 4NQO-induced oral carcinogenesis in mice [35]. When combined with an anti-LAG3 neutralization antibody and Paclitaxel, epacadostat enhanced a therapeutic effect in reducing tumor metastasis in mice [36]. However, its relevance in PCOS remains unexplored. Based on our findings of IDO1 activation in PCOS, we hypothesized that epacadostat could mitigate PCOS-related metabolic and reproductive dysfunctions. Thus, we administered epacadostat in the drinking water at a dose of 2 g L^{-1}, which resulted in a significant reduction in hepatic L-Kyn levels (Fig. 2e), corresponding with IDO1 inhibition by epacadostat (Fig. 3a, b, c). The PCOS-related reproductive and metabolic dysfunctions were alleviated by the epacadostat (Fig. 3f to n, and Extended Data Fig. 2a to c). These findings provide mechanistic insights into the therapeutic potential of IDO1-targeted interventions in PCOS and may help clarify the limited efficacy of epacadostat in clinical trials.

To validate the involvement of L-Kyn in PCOS, we collected human serum samples to comprehensively assess the impact of L-Kyn on PCOS symptoms. Our case-control study, which included 44 control women and 40 PCOS patients, showed that serum Trp and L-Kyn levels did not differ between the two groups (Fig. 4b, c). However, Wang et al. found that plasma Trp and L-Kyn levels are increased in PCOS patients, independent of BMI [18]. Furthermore, existing evidence suggests that obesity is associated with increased circulating Kyn levels [3]. To clarify this discrepancy, we stratified participants into four groups based on BMI. Notably, L-Kyn levels were elevated only in the serum of PCOS patients who were overweight (Fig. 4d). Additionally, KTR analysis indicated that IDO1 activation was specific to obese women with PCOS (Fig. 4f). The divergence between our findings and previous studies may be attributed to variations in populations and their dietary habits. As an essential amino acid, Trp can only be obtained through dietary intake. Therefore, variations in dietary habits due to regional factors, as well as genetic differences among ethnic groups, may influence the digestion, absorption, metabolism, and cellular utilization of amino acids, ultimately affecting the observed results. To further elucidate the metabolic role of L-Kyn in PCOS, we analyzed its relationship with serum lipid profiles. Our results demonstrated a positive correlation between serum L-Kyn and LDL-C levels (Fig. 4g), while an inverse correlation was observed with HDL-C (Fig. 4h). No significant associations were found with TG or TC when analyzing PCOS and control women collectively (Fig. 4i and j). This finding provides the first crucial evidence implicating L-Kyn in the dyslipidemia associated with PCOS.

Collectively, our findings highlight the significant role of IDO1 in both ovarian steroidogenesis and metabolic dysregulation, suggesting its potential as a therapeutic target for PCOS. Exogenous L-Kyn administration disrupted the estrous cycle, altered ovary morphology, and exacerbated IR and hyperlipidemia, similar to those observed in the LET dose (Fig. 4m, n, o, p, and Extended Data Fig. 3a, b, c, d, and f). This aligns with previous studies demonstrating that L-Kyn can induce insulin resistance in mice [3]. Interestingly, L-Kyn did not influence serum T levels (Fig. 4l), which is consistent with our observation that serum L-Kyn levels were not positively correlated with T levels in patients (Extended Data Fig. 3e). This further supports the hypothesis that L-Kyn contributes to PCOS pathogenesis predominantly through metabolic rather than direct steroid hormone synthesis. The previous study illustrates that free Trp and its metabolites, L-Kyn, bind to albumin in the intestinal epithelium and are subsequently transported into the liver via circulation [37]. However, the metabolic pathways of exogenous L-Kyn following subcutaneous injection remain unexplored. Thus, we speculate the differential effects on T levels between the L-Kyn and LET mouse models may be due to higher hepatic accumulation of L-Kyn rather than direct ovarian effects. The increased levels of L-Kyn in the liver trigger severe dyslipidemia, which in turn promotes IR and abnormal cytokine secretion, ultimately impairing ovary function and contributing to ovulatory obstacles. Since L-Kyn itself does not directly affect the ovary

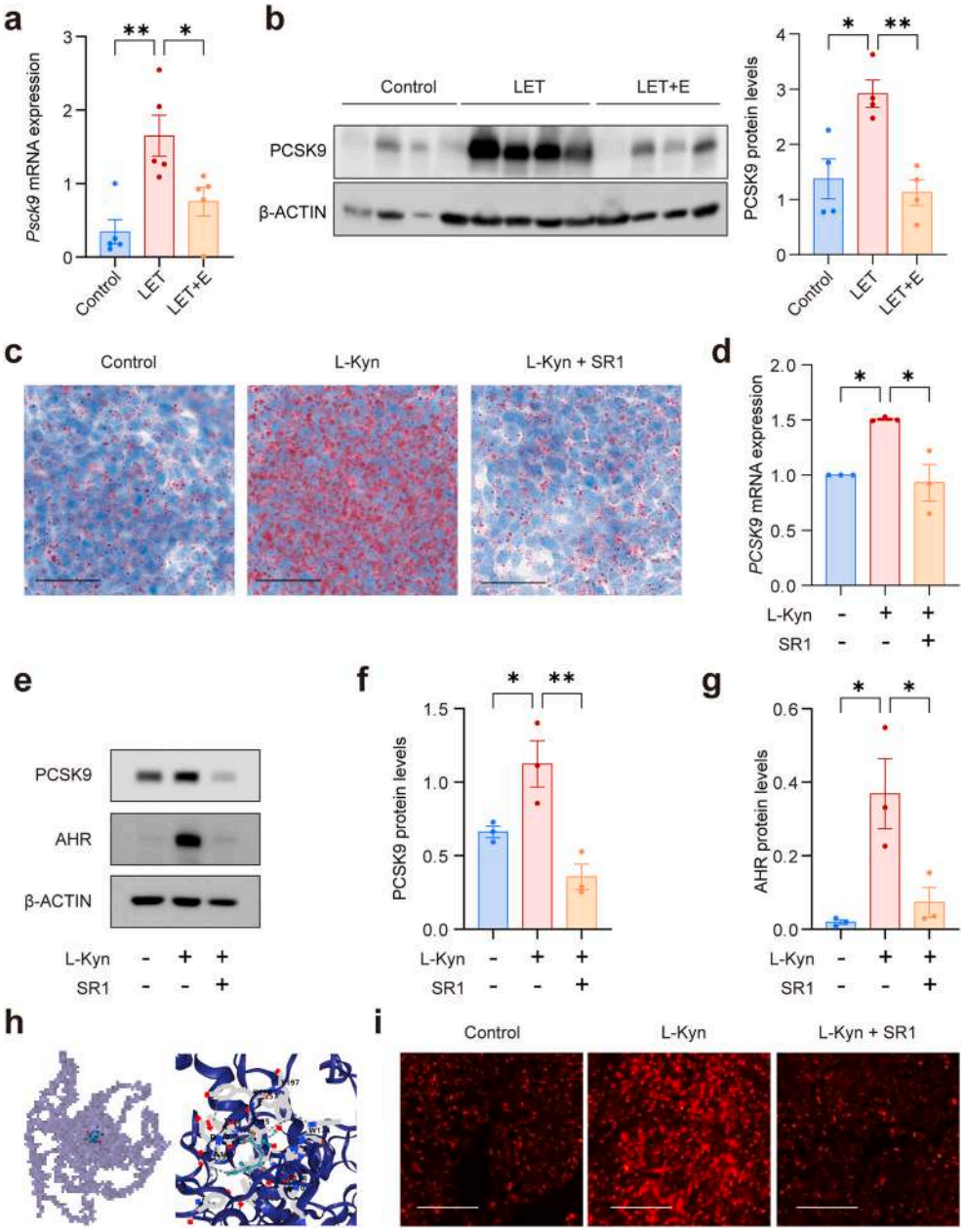

Fig. 5. IDO1-catalyzed L-Kyn exacerbates dyslipidemia via the AHR-PCSK9 axis in PCOS. a, Relative mRNA expressions of *Pcsk9* in the liver from mice in the indicated groups (n = 5 mice per group). b, Protein levels of PCSK9 in the liver from mice in the indicated groups (n = 4 mice per group). c, Oil Red staining of lipid droplets within the hepG2 cells, bar = 50 μm. d, Relative mRNA expressions of *PCSK9* in the hepG2 cells (*n* = 3 per group). e, Western blot analysis of AHR and PCSK9 in hepG2 cells (n = 3 per group). f, Relative protein levels of PCSK9 in the hepG2 cells (n = 3 per group). g, Relative protein levels of AHR in the hepG2 cells (n = 3 per group). h, Docking model of the L-Kyn and AHR. i, Image of LDL-C absorption in hepG2, bar = 50 μm. *p* values were determined by one-way ANOVA with Tukey's multiple comparisons post-hoc test, and data were presented as means ± SEM. $^{*}p < 0.05$, $^{**}p < 0.01$.

and its accumulation is insufficient to impair ovarian cell function, T production remains unaffected. Furthermore, PCOS arises from the complex interplay of HA, obesity, abdominal adiposity, and IR [38]. Evidence suggests that HA is the central defect in PCOS, while obesity, abdominal adiposity, and IR serve as common triggers or modifiers of the condition [39]. The phenotypic divergence observed between lean and obese PCOS patients can be attributed to the varying contributions of these factors across individuals. This explains the clinical heterogeneity of PCOS. In lean PCOS patients, the severity of HA alone without IR and obesity can be sufficient to induce the full spectrum of PCOS manifestations. In contrast, in obese PCOS patients, obesity-related metabolic disturbances may exacerbate even modest androgen overproduction, contributing to the manifestation of PCOS. This mechanistic framework also explains the partial reversibility of PCOS features following significant weight loss. Our experimental findings also support this framework. Exogenous administration of L-Kyn induced PCOS-like features, including disrupted estrous cyclicity, polycystic ovarian morphology, lipid dysmetabolism, and glucose intolerance, in mice without elevating T levels (Fig. 4l, m, n, and o, Extended Data Fig. 3a, b, c, d, and f). This finding highlights that metabolic disturbances can trigger the pathophysiology of PCOS, even in the absence of overt hyperandrogenism. Studies in *Ido1* knockout mice provided compelling evidence that *Ido1* upregulation-induced excessive L-Kyn resulted in disrupted estrous cycles, polycystic ovary morphology, and hepatic lipid accumulation (Extended Data Fig. 3a, b, c, d, i and j). Particularly, LET failed to induce hyperandrogenemia in the absence of

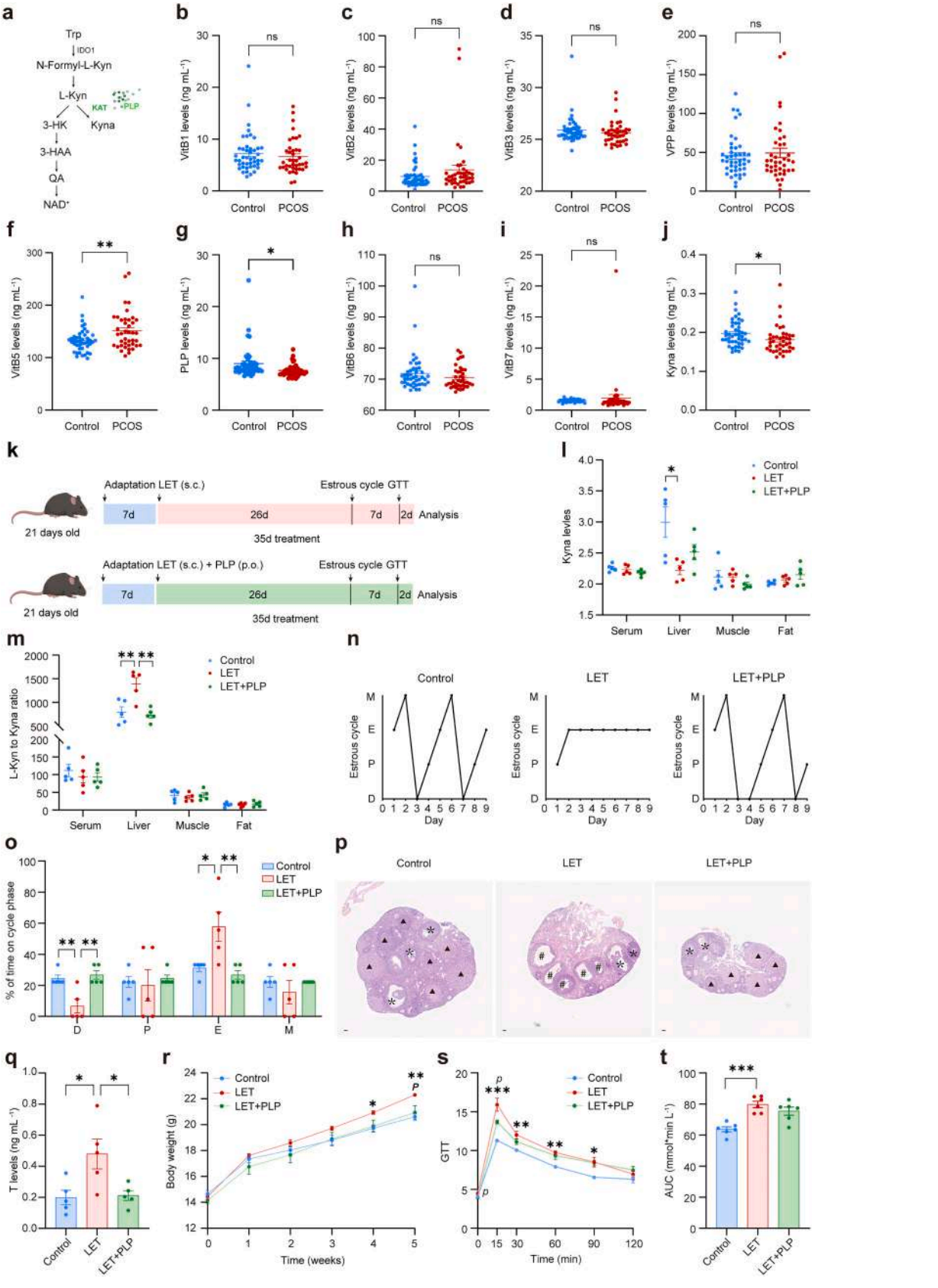

(caption on next page)

Fig. 6. PLP ameliorates PCOS by promoting L-Kyn catabolite to Kyna. a, The KP pathway schedule. b, c, d, e, f, g, h, and i, Serum VitB1, VitB2, VitB3, VPP, VitB5, PLP, VitB6, and VitB7 levels of women with or without PCOS (n = 44 in the Control group, n = 40 in the PCOS group). j, Serum Kyna levels of women with or without PCOS (n = 44 in the Control group, n = 40 in the PCOS group). k, Schematic illustration of the mice model design. The mice were divided into three groups (Control, LET, and LET+PLP). The mice in the control group were treated with PBS for 35 days, while those in the LET group received LET treatment for the same duration. The mice of the LET+PLP group were administered LET and PLP simultaneously for 35 days. l, Serum, liver, muscle, and fat Kyna levels of mice (n = 5 mice per group). The unit of Kyna is expresed in ng mL^{-1} in serum, and in ng g^{-1} in liver, SK and fat tissue. m, Serum, liver, muscle, and fat KTR of mice (n = 5 mice per group). n, Representative estrous cycles. M, metestrus; D, diestrus; P, proestrus; E, estrus. o, Percentage of each stage in estrous cycles (n = 5 mice per group). p, Ovary morphology represented by HE staining. The triangle symbol represents corpus luteum; The asterisk symbol represents atretic follicles; The well number symbol represents cystic follicles. Scale bar: 200 μm. q, Measurement of serum T levels (n = 5 mice per group). r, Body weight changes (n = 6 mice per group). s and t, GTT and AUC (n = 6 mice per group). For b, c, d, e, f, g, h, i, j, *p* values were determined by unpaired-*t*-test. $*p < 0.05$; $**p < 0.01$. For l, m, o, q and t, *p* values were determined by one-way ANOVA with Tukey's multiple comparisons post-hoc test, and data were presented as means ± SEM. $*p < 0.05$; $**p < 0.01$; $***p < 0.001$. For r and s, *p* values were determined by one-way ANOVA with Tukey's multiple comparisons post-hoc test, and data were presented as means ± SEM. $*p < 0.05$, $**p < 0.01$, $***p < 0.001$, Control versus the LET group. $^{p}p < 0.05$, LET versus the LET+PLP group.

Ido1 (Extended Data Fig. 3h). In contrast, exogenous L-Kyn administration restored T production of *Ido1*$^{-/-}$ mice, indicating that while L-Kyn itself does not directly stimulate androgen synthesis, it is essential for LET-mediated hyperandrogenism.

The lipid-decreasing effect of epacadostat indicates that L-Kyn may serve as a promising target for dyslipidemia intervention in PCOS. PCSK9 is a highly conserved enzyme responsible for regulating cholesterol homeostasis by promoting the degradation of LDL receptors, leading to excessive LDL-C accumulation [27]. However, the factors driving PCSK9 upregulation in PCOS remain unclear. Here, we uncovered a novel role of L-Kyn in modulating LDL-C levels through the lipid metabolic regulator PCSK9. We observed that *Pcsk9* mRNA expression and PCSK9 protein levels were increased in the liver of the PCOS mice but significantly reduced following IDO1 inhibition by epacadostat (Fig. 5a, b). This is consistent with a previous study that PCSK9 inhibition reduces circulating TC and LDL-C levels in PCOS mice [27]. However, our study is the first to report that L-Kyn directly regulates PCSK9. Our in vitro experiments further demonstrated that L-Kyn enhances PCSK9 at both the mRNA and protein levels, leading to an increased LDL uptake capacity in HepG2 cells (Fig. 5c, d, e, f, and i). A previous study reported that L-Kyn promotes AHR translocation into the nucleus, facilitating the transcription of target genes [28]. Consistently, our results revealed increased AHR expression in HepG2 cells stimulated with L-Kyn compared to control cells (Fig. 5e, g). Notably, the enhancement of LDL uptake by L-Kyn was reversed by co-administration of SR1, an inhibitor of AHR (Fig. 5i). Collectively, these findings emphasize the crucial role of the L-Kyn-AHR-PCSK9 pathway in the dyslipidemia associated with PCOS.

Kyna is a downstream metabolite of L-Kyn catabolism. We demonstrated that PCOS patients exhibit significantly lower serum Kyna levels (Fig. 6j). A similar phenomenon was observed in PCOS-like mice, where Kyna levels were significantly reduced in the liver of LET mice (Fig. 6l). PLP acts as a cofactor for key enzymes involved in the catabolic processes of L-Kyn. We first establish that the decrease in PLP levels in PCOS patients aligns with the tendency of Kyna. Notably, PLP supplementation reduced L-Kyn accumulation in the liver of PCOS mice, as evidenced by a decreased L-Kyn to Kyna ratio (Fig. 6m) and the attenuation of PCOS traits (Fig. 6n, o, p, q, r, s, t and Extended Data Fig. 5). Additionally, we found that serum Vit B5 levels were elevated in PCOS patients (Fig. 6f). Previous research has shown that Vnn1 is a pantetheinase that catalyzes the conversion of pantetheine to pantothenate (Vit B5) [40]. Notably, increased expression of Vnn1 in intestinal epithelial cells has been identified as a compensatory response to inflammation in the inflammatory bowel disease (IBD) mouse model. This upregulation of Vnn1 promotes Vit B5 synthesis, which aids in repairing the intestinal mucosal barrier and enhancing the effectiveness of anti-inflammatory treatments. Given that PCOS is also associated with chronic low-grade inflammation, we hypothesize that the elevated serum Vit B5 levels in PCOS patients may similarly represent a compensatory response. Furthermore, no studies have investigated the relationship between Vit B5 and L-Kyn, suggesting that the observed elevation in Vit B5 levels is more likely a compensatory response than a result of changes in Trp metabolism. Another potential explanation involves the MYC oncogene, which has been linked to increased vitamin B5 levels in tumor environments. A study reported that vitamin B5 is enriched in MYC-high regions of both human and murine mammary tumors [41]. This enrichment is driven by MYC-mediated upregulation of solute carrier family 5 member 6 (SLC5A6), a multivitamin transporter, leading to enhanced vitamin B5 uptake and utilization. Additionally, previous research has implicated MYC signaling in PCOS pathophysiology. Specifically, leptin (LEP), which is elevated in the serum and follicular fluid of PCOS patients, activates c-MYC, modulates telomerase reverse transcriptase (TERT) expression, and increases telomerase activity and telomere length, ultimately contributing to granulosa cell apoptosis and ovarian dysfunction. Based on these findings, we propose that the elevated vitamin B5 levels observed in PCOS patients may be linked to MYC pathway activation [42]. These findings suggest that reducing hepatic L-Kyn levels may help prevent PCOS.

Overall, we propose a model wherein L-Kyn promotes PCOS development by modulating androgen levels and lipid metabolism. Epacadostat directly targets IDO1, thereby inhibiting the L-Kyn-AHR-PCSK9 interaction, reducing LDL-C accumulation, and suppressing androgen synthesis. Additionally, PLP ameliorates PCOS traits by promoting L-Kyn metabolizing to Kyna. Our findings highlight the therapeutic effect of epacadostat and PLP in PCOS management. This discovery opens up potential targets for controlling lipid homeostasis by targeting the L-Kyn-AHR-PCSK9 interaction.

These findings indicate that L-Kyn, a key metabolite in the Trp metabolic pathway, exhibits significant abnormalities in women with PCOS and is closely associated with dysregulated lipid metabolism. Given the substantial heterogeneity of PCOS, current clinical diagnosis primarily relies on the Rotterdam criteria, lacking effective biomarkers for risk prediction. The elevated levels of L-Kyn and KTR provide insights into the underlying mechanisms driving PCOS pathogenesis and hold promise as potential metabolic biomarkers for improving early detection and phenotypic classification. Furthermore, the integration of metabolomics-based multi-marker models may enhance diagnostic precision and provide novel strategies for personalized treatment. Future research should further explore the distinct expression patterns of L-Kyn and KTR across PCOS subtypes, as well as their potential utility in therapeutic monitoring and prognostic assessment.

4. Materials and methods

4.1. Human study

A total of 84 serum samples of women were recruited from the Center for Reproductive Medicine at Ren Ji Hospital, and donated by the Reproductive Medical Center at First Affiliated Hospital of Henan University of Science and Technology, China. Serum samples were collected from March 2024 to September 2024. This study was approved by the Ethics Committee of the First Affiliated Hospital of Henan University of Science and Technology (2024–0050) and the Application Form of the ART Bthics Committee (2015071707). The PCOS patients all have at

least two phenotypes according to the 2003 Rotterdam Criteria: I oligo- or an-ovulation; II higher T levels and/or clinical signs indicating hyperandrogenism; III polycystic ovary change (transvaginal ultrasonography detection shows at least 12 antral follicles in each ovary). Other diseases that may influence sex hormones, prolactin (PRL), LH, follicle-stimulating hormone (FSH), T, and estradiol (E_2), were excluded from the study. The control subjects participating with normal hormone levels, ovarian morphology, and regular menstrual cycles were selected from women who were diagnosed with primary or secondary infertility due to oviduct obstruction or male infertility.

4.2. Animal study

21-day-old C57BL/6 mice were purchased from Charles River Laboratories (Beijing, China) and randomly housed 5 per cage. Mice were maintained under specific pathogen-free conditions with stationary temperature (21 °C ± 2 °C), and a lighting schedule of 12 h of light and 12 h of darkness. After 1-week-adaptation, all mice received treatment for 35 days. The mice of the control group were injected daily with 100 μL sesame oil. The mice in the LET group received a daily subcutaneous injection of LET at a dosage of 1 mg kg^{-1} of body weight, dissolved in 100 μL sesame oil. The mice in the L-Kyn group were injected subcutaneously daily with L-Kyn at a dosage of 20 mg kg^{-1} of body weight, dissolved in 100 μL of sesame oil. In the rescue experiments, mice that were injected with LET received simultaneous supplementation of 2 mg mL^{-1} epacadostat or 2 mg mL^{-1} PLP dissolved in the drinking water. The *Ido1* knockout (*Ido1*$^{+/-}$) mice with a C57BL/6 background were obtained from the Cyagen Biosciences. The *Ido1*$^{+/-}$ mice were crossed with each other to generate the homozygous mouse. 21-day-old *Ido1*$^{-/-}$ mice were adapted for 1 week and then were injected with LET with or without L-Kyn for 35 days. Body weight was measured once per week. Before the mice were killed, the mice from each group were conducted the glucose tolerance test (GTT). The estrous cycle was determined by vaginal cytology during the latest 9 consecutive days. All animal experimental procedures were approved by the Experimental Animal Ethics Committee of Shanghai Laisen Original Life Science Co., LTD. (SOP-MAE-006-011).

4.3. Hematoxylin and eosin (HE) staining

Mice ovaries and adipose tissues were collected and immersed in the Universal Tissue Fixative (Neutral) (G1101, Servicebio) and the Fixative Specific for Fat (G1119, Servicebio), respectively. Following this, the samples were placed in 70 % ethanol for dehydration and then embedded in paraffin. The tissues were sliced into 5 μm thick sections, which were subsequently deparaffinized. The prepared sections were then stained with HE. Images of the stained sections were captured using a high-throughput digital slide scanning system (NanoZoomer S360, Hamamatsu).

4.4. Biochemical assessment of T, serum lipid and ifnγ levels

The concentrations of T, TG, TC, HDL-C, LDL-C, and ifnγ of mice were detected using Testosterone rat/mouse ELISA (DEV9911, Demeditec), Triglyceride (TG) Colorimetric Assay Kit (E-BC-K261-M, Elabscience), Total Cholesterol (TC) Colorimetric Assay Kit (E-BC-K109-M, Elabscience), High-density Lipoprotein Cholesterol (HDL-C) Colorimetric Assay Kit (E-BC-K221-M, Elabscience), Low-density Lipoprotein Cholesterol(LDL-C) Assay Kit (E-BC-K205-M, Elabscience), and Mouse Ifn-γ High Sensitivity ELISA Kit (EK280HS, multi sciences) respectively. All procedures followed the recommended instructions provided by the manufacturers of the kits.

4.5. GTT

For the GTT assay, glucose concentrations were initially measured after a 12 h fasting period. Subsequently, the mice were given an intraperitoneal injection of glucose at 2 g kg^{-1} of body weight. Blood samples were collected from the tail vein, and glucose levels were assessed using a glucometer (ACCU-CHEK, Roche, Germany) at 15, 30, 60, 90, and 120 minutes (min) post-injection. The area AUC of each mouse was calculated by the GraphPad Prism 10.

4.6. Oil Red O staining

For Oil Red O staining, the liver tissue was harvested and immersed in 4 % paraformaldehyde and stained with 60 % Oil Red O staining solution. After washing with phosphate buffer saline (PBS), the sections were incubated with 75 % ethanol, followed by staining with hematoxylin for 5 min. HepG2 cells were washed with PBS, and fixed with 4 % paraformaldehyde for 10 min at room temperature. Then, the cells were washed twice with PBS and incubated with dyeing wash provided by the Improved oil red O staining kit (C0158S, Beyotime) for 20 seconds (s). After removing the dyeing wash, the hepG2 cells were incubated with improved oil Red O staining solution for 20 min. Remove the oil red O dyeing working liquid, add an appropriate amount of dyeing washing liquid, leave for 30 s, then remove the dyeing washing liquid, and wash with PBS for 20 s. Pictures were scanned using a high-throughput digital slide scanning system (NanoZoomer S360, Hamamatsu).

4.7. Transmission electron microscope

Fresh liver tissue was cut into 1 mm^3 pieces and fixed in an electron microscope fixative (G1102, Servicebio) at room temperature for 1 h, followed by overnight fixation at 4 °C. The samples were then washed three times in PBS before postfixing with 1 % osmium tetroxide for 2 h at 4 °C. After dehydration in ethanol, the samples were infiltrated and embedded. Subsequently, they were sectioned to approximately 70 nm thickness. The sample sections were mounted on copper grids, stained with lead citrate, and observed using an electron microscope (Hitachi HT7800, Tokyo, Japan).

4.8. LC-MS for Trp metabolism

500 μL extract (water/methanol/acetonitrile =1:2:2, v/v), 10 μL internal standard (2 μg mL^{-1}), and 2 mm zirconia beads were added to 100 mg tissue samples and homogenized in the MP sample preparation equipment for 3 times (20 s each time). Following homogenization, the samples were centrifuged at 4 °C at 14000 relative centrifugal force (rcf) for 15 min. After centrifugation, 400 μL of the supernatant was transferred to an HLP plate, and the filtered liquid was collected for subsequent testing. For the serum sample preparation, 400 μL of the extract (with the same water/methanol/acetonitrile ratio) and 10 μL of the internal standard were added to 100 μL of serum and mixed thoroughly by vortexing for 30 s. The serum samples were then centrifuged at 4 °C at 14000 rcf for 15 min. After centrifugation, 400 μL of the supernatant was transferred to an HLP plate, and the filtered liquid was collected for subsequent analysis. Both the tissue and serum samples were analyzed using the 5500 QTRAP mass spectrometer (SCIEX) in positive and negative ion modes. The positive ion conditions for the 5500 QTRAP ESI source were set as follows: source temperature at 450 °C; Ion Source Gas 1 (Gas1) at 45; Ion Source Gas 2 (Gas2) at 45; Curtain Gas (CUR) at 40; and Ion Spray Voltage Floating (ISVF) at 4500 V. The retention time was adjusted using the standard of the target substance, and metabolite identification was then carried out.

4.9. RNA isolation and quantitative real-time PCR (q-RT-PCR)

Total RNA was isolated from liver tissue using RNAeasy™ Animal RNA Extraction Kit (Centrifugal column) (R0027, Beyotim) following the standard protocol of the constructor. Real-time PCR was carried out after the total RNA was extracted and reverse transcribed to cDNA using

PrimeScript™ RT Master Mix (Perfect Real Time) (RR036A, Takara) according to the manufacturer's instructions. qRT-PCR experiments were conducted in triplicate, utilizing 60 ng of cDNA per reaction and 10 μM of forward and reverse primers. The reactions were carried out with SYBR® Green Realtime PCR Master Mix (QPK-201, TOYOBO) on the applied biosystems QuantStudio 7 Flex (Thermo Fisher Scientific). The primers and their corresponding sequences are enlisted in the Extended Data Table 2. The expression levels of the target genes were normalized to β-actin, and the expression of the target genes was calculated using the $2^{-\Delta\Delta CT}$ method. The control group was used for normalization.

4.10. Western blot analysis

Cells and tissues were lysed in RIPA buffer (PC101, Epizyme) containing Phosphatase Inhibitor Mixture (GRF102, Epizyme) and Protease Inhibitor Mixture (GRF101, Epizyme). Protein samples were separated with SDS-PAGE and transferred onto the PVDF membrane (IPVH00010, Merck). After blocking with 5 % non-fat milk, the membrane was incubated with diluted IDO1 antibody (1:1000; 654001, Biolegend), β-ACTIN antibody (1:20000, 66009-1, Proteintech), PCSK9 antibody (1,1000, ab181142, Abcam) and AHR antibody (1,1000, ab190797, Abcam) overnight at 4 °C. Then, HRP-conjugated secondary antibodies (1,5000) were incubated for 1.5 h at room temperature. β-ACTIN was used for normalization, and the intensity of each reactive band was analyzed using Image J.

4.11. Cell culture and treatment

The hepG2 cell line was obtained from a Cell Resource Center (Shanghai Institutes for Biological Sciences, Chinese Academy of Sciences). HepG2 cells were cultured in high glucose-DMEM/F12 (11965-092, Gibco) supplemented with 10 % fetal bovine serum (FBS) (C04001, VivaCell) at 37 °C in a humidified atmosphere, with 5 % CO2. The cell lines were routinely subcultured every 2 or 3 days. For the stimulated experiment, L-Kyn sulfate (K3750, Sigma) was added to the medium for 24 h. For the rescue experiment, 1 μM SR1 (S2858, Selleck) was added into the medium for 24 h. For the LDL-C absorption experiment, after being treated with L-Kyn with or without SR1, hepG2 cells underwent a 24 h starvation in the high-glucose DMEM/F12 without FBS, followed by stimulating with 40 μg mL^{-1} Dil-LDL (20614ES76, YEASEN) dissolve in high-glucose DMEM/F12 without FBS for 4 h. Afterward, the Dil-LDL solution was discarded, and the hepG2 cells were washed three times with PBS. Images were then captured using a Zeiss microscope.

4.12. Statistical analysis

Results are presented as means ± standard error of the mean (SEM). Statistical analyses were conducted using IBM SPSS version 29.0. The *one-way analysis of variance (ANOVA)* followed by *Tukey's post-hoc test* was used to assess the statistical significance of differences among three or more groups. The *unpaired t-test* was employed to evaluate the significance between the two groups. The *p*-value of <0.05 was considered statistically significant. The correlation between the serum lipids and L-Kyn levels was analyzed using the *nonparametric Spearman's test*. For the basic index of the women, the data were represented by the median (interquartile range). *Independent sample t-test* and the *Mann-Whitney U test* were used for normally and non-normally distributed variables, respectively.

CRediT authorship contribution statement

Yujiao Wang: Writing – review & editing, Writing – original draft, Visualization, Validation, Supervision, Software, Resources, Project administration, Methodology, Investigation, Formal analysis, Data curation. **Yifan Wu:** Methodology, Conceptualization. **Hongwei Jiang:** Resources. **Shang Li:** Supervision, Project administration, Methodology. **Jingjing Li:** Resources. **Cong Wang:** Methodology. **Lexin Yang:** Writing – review & editing, Methodology. **Xiying Zhou:** Writing – review & editing, Conceptualization. **Juanjuan Yu:** Methodology. **Junyu Zhai:** Supervision, Methodology. **Zi-Jiang Chen:** Supervision. **Yanzhi Du:** Writing – review & editing, Supervision, Project administration, Funding acquisition.

Declaration of competing interest

The authors declare that they have no known competing financial interests or personal relationships that could have appeared to influence the work reported in this paper.

Acknowledgments

This work was supported by grants from the National Key Research and Development Program of China (No. 2024YFC2706703 and 2022YFC2703204), National Natural Science Foundation of China (No. 82171623 and 81971343), Innovative Research Team of High-Level Local Universities in Shanghai (No. SHSMU-ZLCX20210200), and Shanghai Commission of Science and Technology (No. 21XD1401900 and 20DZ2270900).

Appendix A. Supplementary data

Supplementary data to this article can be found online at https://doi.org/10.1016/j.metabol.2025.156238.

References

[1] Joham AE, Norman RJ, Stener-Victorin E, Legro RS, Franks S, Moran LJ, et al. Polycystic ovary syndrome. Lancet Diabetes Endocrinol 2022;10(9):668–80. https://doi.org/10.1016/S2213-8587(22)00163-2.
[2] McCartney CR, Marshall JC. Polycystic ovary syndrome. N Engl J Med 2016;375(1):54–64. https://doi.org/10.1056/NEJMcp1514916.
[3] Huang T, Song J, Gao J, Cheng J, Xie H, Zhang L, et al. Adipocyte-derived kynurenine promotes obesity and insulin resistance by activating the AhR/STAT3/IL-6 signaling. Nat Commun 2022;13(1):3489. https://doi.org/10.1038/s41467-022-31126-5.
[4] Liu Y, Jiang J, Du S, Mu L, Fan J, Hu J, et al. Artemisinins ameliorate polycystic ovarian syndrome by mediating LONP1-CYP11A1 interaction. Science 2024;384(6701):eadk5382. https://doi.org/10.1126/science.adk5382.
[5] Anagnostis P, Tarlatzis BC, Kauffman RP. Polycystic ovarian syndrome (PCOS): long-term metabolic consequences. Metab Clin Exp 2018. https://doi.org/10.1016/j.metabol.2017.09.016.
[6] Wekker V, Van Dammen L, Koning A, Heida KY, Painter RC, Limpens J, et al. Long-term cardiometabolic disease risk in women with PCOS: a systematic review and meta-analysis. Hum Reprod Update 2020;26(6):942–60. https://doi.org/10.1093/humupd/dmaa029.
[7] Zhang C, Li Y, Wang Y, Hu S, Liu Y, Liang X, et al. Genetic associations of metabolic factors and therapeutic drug targets with polycystic ovary syndrome. J Adv Res 2024:S2090123224004922. https://doi.org/10.1016/j.jare.2024.10.038.
[8] Li S, Zhai J, Chu W, Geng X, Wang D, Jiao L, et al. Alleviation of *Limosilactobacillus reuteri* in polycystic ovary syndrome protects against circadian dysrhythmia-induced dyslipidemia via capric acid and GALR1 signaling. Npj Biofilms Microbiomes 2023;9(1):47. https://doi.org/10.1038/s41522-023-00415-2.
[9] Hu Z, Wang Y, Qiao J, Li M, Chi H, Chen X. The role of family history in clinical symptoms and therapeutic outcomes of women with polycystic ovary syndrome. Int J Gynecol Obstet 2010;108(1):35–9. https://doi.org/10.1016/j.ijgo.2009.08.004.
[10] Nichols AR, Chavarro JE, Oken E. Reproductive risk factors across the female lifecourse and later metabolic health. Cell Metab 2024;36(2):240–62. https://doi.org/10.1016/j.cmet.2024.01.002.
[11] Wang X, Han H, Shi X, Nie X, Zhu R, Jin J, et al. Genetic insights of blood lipid metabolites on polycystic ovary syndrome risk: a bidirectional two-sample Mendelian randomization study. Front Endocrinol 2024;15:1391826. https://doi.org/10.3389/fendo.2024.1391826.
[12] Qian Y, Tong Y, Zeng Y, Huang J, Liu K, Xie Y, et al. Integrated lipid metabolomics and proteomics analysis reveal the pathogenesis of polycystic ovary syndrome. J Transl Med 2024;22(1):364. https://doi.org/10.1186/s12967-024-05167-x.
[13] Wang TJ, Larson MG, Vasan RS, Cheng S, Rhee EP, McCabe E, et al. Metabolite profiles and the risk of developing diabetes. Nat Med 2011;17(4):448–53. https://doi.org/10.1038/nm.2307.
[14] Wu J, Wang K, Wang X, Pang Y, Jiang C. The role of the gut microbiome and its metabolites in metabolic diseases. Protein Cell 2021;12(5):360–73. https://doi.org/10.1007/s13238-020-00814-7.

[15] He Y, Shi L, Qi Y, Wang Q, Zhao J, Zhang H, et al. Butylated starch alleviates polycystic ovary syndrome by stimulating the secretion of peptide tyrosine-tyrosine and regulating faecal microbiota. Carbohydr Polym 2022;287:119304. https://doi.org/10.1016/j.carbpol.2022.119304.
[16] Qi X, Yun C, Sun L, Xia J, Wu Q, Wang Y, et al. Gut microbiota–bile acid–interleukin-22 axis orchestrates polycystic ovary syndrome. Nat Med 2019;25(8):1225–33. https://doi.org/10.1038/s41591-019-0509-0.
[17] Mu L, Ye Z, Hu J, Zhang Y, Chen K, Sun H, et al. PPM1K-regulated impaired catabolism of branched-chain amino acids orchestrates polycystic ovary syndrome. eBioMedicine 2023;89:104492. https://doi.org/10.1016/j.ebiom.2023.104492.
[18] Wang S, Mu L, Zhang C, Long X, Zhang Y, Li R, et al. Abnormal activation of tryptophan-kynurenine pathway in women with polycystic ovary syndrome. Front Endocrinol 2022;13:877807. https://doi.org/10.3389/fendo.2022.877807.
[19] Xue C, Li G, Zheng Q, Gu X, Shi Q, Su Y, et al. Tryptophan metabolism in health and disease. Cell Metab 2023;35(8):1304–26. https://doi.org/10.1016/j.cmet.2023.06.004.
[20] Chajadine M, Laurans L, Radecke T, Mouttoulingam N, Al-Rifai R, Bacquer E, et al. Harnessing intestinal tryptophan catabolism to relieve atherosclerosis in mice. Nat Commun 2024;15(1):6390. https://doi.org/10.1038/s41467-024-50807-x.
[21] Sinclair LV. Single cell analysis of kynurenine and system L amino acid transport in T cells. Nat Commun 2018. https://doi.org/10.1038/s41467-018-04366-7.
[22] Pires AS, Sundaram G, Heng B, Krishnamurthy S, Brew BJ, Guillemin GJ. Recent advances in clinical trials targeting the kynurenine pathway. Pharmacol Ther 2022;236:108055. https://doi.org/10.1016/j.pharmthera.2021.108055.
[23] Seo S-K, Kwon B. Immune regulation through tryptophan metabolism. Exp Mol Med 2023;55(7):1371–9. https://doi.org/10.1038/s12276-023-01028-7.
[24] Agudelo LZ, Femenía T, Orhan F, Porsmyr-Palmertz M, Goiny M, Martinez-Redondo V, et al. Skeletal muscle PGC-1α1 modulates kynurenine metabolism and mediates resilience to stress-induced depression. Cell 2014;159(1):33–45. https://doi.org/10.1016/j.cell.2014.07.051.
[25] Priyadarshini M, Navarro G, Reiman DJ, Sharma A, Xu K, Lednovich K, et al. Gestational insulin resistance is mediated by the gut microbiome–indoleamine 2,3-dioxygenase axis. Gastroenterology 2022;162(6):1675–1689.e11. https://doi.org/10.1053/j.gastro.2022.01.008.
[26] Rodgers RJ, Irving-Rodgers HF. Formation of the ovarian follicular antrum and follicular fluid1. Biol Reprod 2010;82(6):1021–9. https://doi.org/10.1095/biolreprod.109.082941.
[27] Wang M, Zhao D, Xu L, Guo W, Nie L, Lei Y, et al. Role of PCSK9 in lipid metabolic disorders and ovarian dysfunction in polycystic ovary syndrome. Metabolism 2019;94:47–58. https://doi.org/10.1016/j.metabol.2019.02.002.
[28] Lee LY-H, Oldham WM, He H, Wang R, Mulhern R, Handy DE, et al. Interferon-γ impairs human coronary artery endothelial glucose metabolism by tryptophan catabolism and activates fatty acid oxidation. Circulation 2021;144(20):1612–28. https://doi.org/10.1161/CIRCULATIONAHA.121.053960.
[29] Song P, Ramprasath T, Wang H, Zou M-H. Abnormal kynurenine pathway of tryptophan catabolism in cardiovascular diseases. Cell Mol Life Sci 2017;74(16):2899–916. https://doi.org/10.1007/s00018-017-2504-2.
[30] Ling Z-N, Jiang Y-F, Ru J-N, Lu J-H, Ding B, Wu J. Amino acid metabolism in health and disease. Signal Transduct Target Ther 2023;8(1):345. https://doi.org/10.1038/s41392-023-01569-3.
[31] Mimouni NEH, Paiva I, Barbotin A-L, Timzoura FE, Plassard D, Le Gras S, et al. Polycystic ovary syndrome is transmitted via a transgenerational epigenetic process. Cell Metab 2021;33(3):513–30. e8, https://doi.org/10.1016/j.cmet.2021.01.004.
[32] Venkateswaran N, Lafita-Navarro MC, Hao Y-H, Kilgore JA, Perez-Castro L, Braverman J, et al. MYC promotes tryptophan uptake and metabolism by the kynurenine pathway in colon cancer. Genes Dev 2019;33(17–18):1236–51. https://doi.org/10.1101/gad.327056.119.
[33] De Medeiros SF, Rodgers RJ, Norman RJ. Adipocyte and steroidogenic cell cross-talk in polycystic ovary syndrome. Hum Reprod Update 2021;27(4):771–96. https://doi.org/10.1093/humupd/dmab004.
[34] Pan X, Liu Y, Liu L, Pang B, Sun Z, Guan S, et al. Bushen Jieyu Tiaochong formula reduces apoptosis of granulosa cells via the PERK-ATF4-CHOP signaling pathway in a rat model of polycystic ovary syndrome with chronic stress. J Ethnopharmacol 2022;292:114923. https://doi.org/10.1016/j.jep.2021.114923.
[35] Zhang Y, Zhang J, Zhao S, Xu Y, Huang Y, Liu S, et al. Single-cell RNA sequencing highlights the immunosuppression of IDO1^{+} macrophages in the malignant transformation of oral leukoplakia. Theranostics 2024;14(12):4787–805. https://doi.org/10.7150/thno.99112.
[36] Zahraeifard S, Xiao Z, So JY, Ahad A, Montoya S, Park WY, et al. Loss of tumor suppressors promotes inflammatory tumor microenvironment and enhances LAG3+T cell mediated immune suppression. Nat Commun 2024;15(1):5873. https://doi.org/10.1038/s41467-024-50262-8.
[37] Mouttoulingam N, Taleb S. Exploring tryptophan metabolism in cardiometabolic diseases. Trends Endocrinol Metab 2024. https://doi.org/10.1016/j.tem.2024.11.009. S1043276024003175.
[38] Escobar-Morreale HF. Polycystic ovary syndrome: definition, aetiology, diagnosis and treatment. Nat Rev Endocrinol 2018;14(5):270–84. https://doi.org/10.1038/nrendo.2018.24.
[39] Escobar-Morreale HF, Millán JLS. Abdominal adiposity and the polycystic ovary syndrome. Trends Endocrinol Metab 2007;18(7):266–72. https://doi.org/10.1016/j.tem.2007.07.003.
[40] Millet V, Gensollen T, Maltese M, Serrero M, Lesavre N, Bourges C, et al. Harnessing the Vnn1 pantetheinase pathway boosts short chain fatty acids production and mucosal protection in colitis. Gut 2023;72(6):1115–28. https://doi.org/10.1136/gutjnl-2021-325792.
[41] Kreuzaler P, Inglese P, Ghanate A, Gjelaj E, Wu V, Panina Y, et al. Vitamin B5 supports MYC oncogenic metabolism and tumor progression in breast cancer. Nat Metab 2023;5(11):1870–86. https://doi.org/10.1038/s42255-023-00915-7.
[42] Feijing Z, Sun Z, Cheng L, Dong Y. Leptin modulates ovarian granulosa cell apoptosis by regulating telomerase activity and telomere length in polycystic ovary syndrome. Lab Invest 2025;105(2):102169. https://doi.org/10.1016/j.labinv.2024.102169.